DYNAMICS AND CONTROL OF A GYROSCOPE-STABILIZED PLATFORM IN A SELF-PROPELLED ANTI-AIRCRAFT SYSTEM

ZBIGNIEW KORUBA
ZBIGNIEW DZIOPA
IZABELA KRZYSZTOFIK

Kielce University of Technology, Faculty of Mechatronics and Machine Building, Kielce, Poland
e-mail: ksmzko@tu.kielce.pl; zdziopa@tu.kielce.pl; pssik@tu.kielce.pl

The paper presents a mathematical model of a triaxial gyroscopic platform on a moving platform base (motor vehicle). Control software platforms are designated with the inverse dynamics of the duties, while the control correction – using the LQR method. The considered platform can be used as an independent observation base for systems, cameras, parcels or gun machines. In the present study, it is shown in its application to stabilization of anti-aircraft missile launchers.

Key words: antiaircraft system, gyroscope, dynamics and control, gyroscope-stabilized platform

1. A physical model of a launcher in a self-propelled anti-aircraft missile system

Military vehicles require versatile equipment to perform numerous tasks, for instance, observation devices including television and infrared cameras and weapon such as guns, missile launchers, etc. It is essential that reliable reference systems be used to maintain the equipment and weapon constant orientation and effective operation, irrespective of external disturbances such as the vehicle motion.

In this study, we consider a three-axis gyroscope platform employed to angularly stabilize a launcher in a self-propelled missile system.

The launcher mounted on a vehicle consists of two main parts (Dziopa, 2004-2008). One is a pedestal placed directly on the vehicle. The basic motion of the pedestal is very much dependent on that of the carrier. The other

element is a turret mounted on the pedestal. Therefore, the turret basic motion is a combination of the basic motion of the vehicle and the motion of the turret resulting from target detection and tracking processes. There is a thermovision camera fixed on the turret which sends images to the operator's control desk. Sitting in the vehicle in front of a monitor screen, he determines the motion of the turret. The turret consists of two main elements: a platform and a system of four guide rails to launch four missiles. The guide rails are fixed on the platform, symmetrically in relation to a vertical plane passing through the centre of the turret mass. On each side of this plane, there are two guide rails, one above the other. The platform can rotate in relation to the pedestal in accordance with the angle of azimuth ψ_{pv}, where ψ_{pv} is an angle of the platform deviation. The guide rail system is mounted on the platform and together they form a kinematic rather than rotary pair. The guide rail system, therefore, can rotate in relation to the base in accordance with the elevation angle ϑ_{pv}. This angle, ϑ_{pv}, is the angle of pitch of the guide rail system. After the platform and the guide rail system move to the position of target interception, the launcher does not change its configuration. The analysis of the system performance commences on target interception, therefore, in the assumed model the basic motion of the launcher is reduced to the basic motion of the carrier. This means that the basic motion of the launcher is closely related to the basic motion of the vehicle. The turret is an object with inertial characteristic dependent on the target position with respect to the anti-aircraft system. The turret mass remains stable, yet the moments of inertia and the moment of deviation change. Once the target is locked on, the turret characteristic remains unchanged.

The launcher was modelled as two basic masses and eight deformable elements (Fig. 1).

To improve the legibility of the diagram in Fig. 1, the launcher does not include the guide rail system. Figure 2, then, is a supplement of Fig. 1.

The pedestal is a perfectly stiff body with mass m_w and moments of inertia I_{wx} and I_{wz}. The pedestal is mounted to the vehicle body by means of four passive elastic-damping elements with linear parameters k_{w11} and c_{w11}, k_{w12} and c_{w12}, k_{w13} and c_{w13}, and k_{w14} and c_{w14}, respectively. The turret is a perfectly stiff body with mass m_v, moments of inertia I_{vx} and I_{vz} and moment of deviation I_{vxz}. It is mounted to the pedestal by means of four passive elastic-damping elements with linear parameters k_{w21} and c_{w21}, k_{w22} and c_{w22}, k_{w23} and c_{w23}, and k_{w24} and c_{w24}, respectively. The inertial characteristic of the turret is dependent on the actual position of its component objects, i.e. the platform and the guide rail system. The platform is a perfectly stiff body
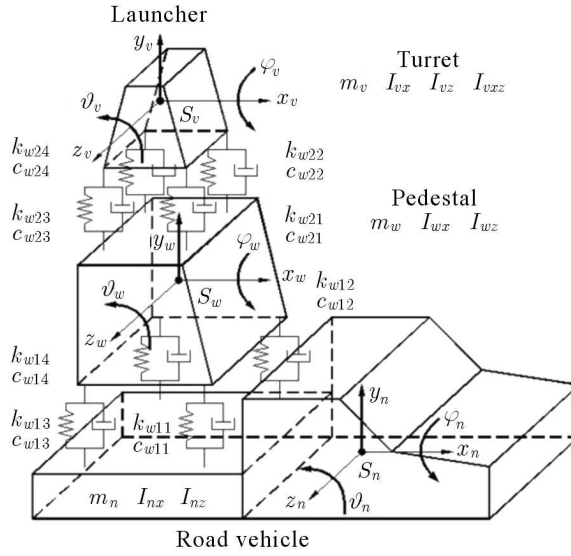
Fig. 1. A physical model of the launcher
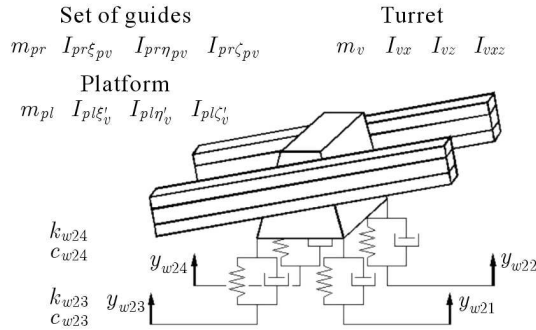
Fig. 2. A physical model of the guide rails

with mass m_{pl} and main central moments of inertia $I_{pl\xi'_v}$, $I_{pl\eta'_v}$, $I_{pl\zeta'_v}$. The four-guide-rail system is also a perfectly stiff body with mass m_{pr} and main central moments of inertia $I_{pr\xi_{pv}}$, $I_{pr\eta_{pv}}$, $I_{pr\zeta_{pv}}$.

The positions of the body of the pedestal with mass m_w and moments of inertia I_{wx} and I_{wz} and those of the body of the turret with mass m_v, moments of inertia I_{vx} and I_{vz} and moment of deviation I_{vxz}, at any moment are determined in right-handed Cartesian orthogonal coordinate systems. The reference systems are as follows:

a) Coordinate systems determining motion of the pedestal:

$0_w x_w y_w z_w$ – the coordinate system moving in the basic motion with respect to the ground-fixed coordinate system $0xyz$. The condition that the cor-

responding axes $0_w x_w \| 0x$, $0_w y_w \| 0y$ and $0_w z_w \| 0z$ are parallel is always satisfied. If the basic motion of the pedestal is not disturbed, then the point 0_w coincides with the centre of pedestal mass at any moment.

$S_w x_w y_w z_w$ – the coordinate system moving, in a general case, in translatory motion with respect to the $0_w x_w y_w z_w$ coordinate system. The origin of the coordinate system S_w coincides with the centre of pedestal mass at any moment. The condition that the corresponding axes $S_w x_w \| 0_w x_w$, $S_w y_w \| 0_w y_w$ and $S_w z_w \| 0_w z_w$ are parallel is always satified. Disturbances to the basic motion cause that the centre of pedestal mass S_w moves along the $0_w y_w$ axis, which means that the translatory motion in the assumed model is reduced to a straight-line motion.

$S_w \xi_w \eta_w \zeta_w$ – the coordinate system moving, in a general case, in rotary motion about a fixed point with respect to the $S_w x_w y_w z_w$ coordinate system. The axes $S_w \xi_w$, $S_w \eta_w$ and $S_w \zeta_w$ are rigidly connected with the pedestal body as they are its main central axes of inertia. Disturbances to the basic motion cause that the pedestal body rotates about the $S_w z_w$ axis in accordance with a change in the pitch angle ϑ_w and about the $S_w x_w$ axis in accordance with a change in the tilt angle φ_w, which means that the rotary motion about a fixed point in the assumed model is reduced to two rotary motions.

If there are no disturbances to the basic motion of the pedestal, then the coordinate systems $0_w x_w y_w z_w$, $S_w x_w y_w z_w$ and $S_w \xi_w \eta_w \zeta_w$ coincide at any moment. In the model, the pedestal is an element of a 3D vibrating system, which perfoms complex motion in relation to the $0_w x_w y_w z_w$ coordinate system. This motion is a combination of a straight-line motion of the centre of mass S_w in accordnace with a change in the y_w coordinate, rotary motion about the $S_w z_w$ axis in accordance with a change in the pitch angle ϑ_w and rotary motion about the $S_w x_w$ axis in accordance with a change in the tilt angle φ_w.

b) Coordinate systems determining motion of the turret:

$0_v x_v y_v z_v$ – the coordinate system performing the basic motion in relation to the ground-fixed coordinate system $0xyz$. The condition that the corresponding axes $0_v x_v \| 0x$, $0_v y_v \| 0y$ and $0_v z_v \| 0z$ are parallel is always satisfied. If there are no disturbances to the basic motion of the pedestal, then the point 0_v coincides with the centre of pedestal mass at any moment.

$S_v x_v y_v z_v$ – the coordinate system performing, in a general case, translatory motion in relation to the $0_v x_v y_v z_v$ coordinate system. The origin of

the coordinate system S_v coincides with the centre of the turret mass at any moment. The condition that the corresponding axes $S_v x_v \| 0_v x_v$, $S_v y_v \| 0_v y_v$ and $S_v z_v \| 0_v z_v$ are parallel is always satified. Disturbances to the basic motion cause that the mass centre of the turret S_v moves along the $0_v y_v$ axis, which means that in the assumed model, the translatory motion is reduced to a straight line motion.

$S_v \xi_v \eta_v \zeta_v$ – the coordinate system moving, in a general case, in rotary motion about a fixed point in relation to the $S_v x_v y_v z_v$ coordinate system. The $S_v \xi_v$, $S_v \eta_v$ and $S_v \zeta_v$ axes are rigidly connected with the turret body as they are the main central axes of inertia if the following conditions are met: $\psi_{pv} = 0$ and $\vartheta_{pv} = 0$. Disturbances to the basic motion cause that the turret body rotates about the $S_v z_v$ axis in accordance with a change in the pitch angle ϑ_v and about the $S_v x_v$ axis in accordance with a change in the tilt angle φ_v, which means that, in the assumed model, the rotary motion about a fixed point is reduced to two rotary motions.

If there are no disturbances to the basic motion of the turret, the coordinate systems $0_v x_v y_v z_v$, $S_v x_v y_v z_v$ and $S_v \xi_v \eta_v \zeta_v$ coincide at any moment. In the model, the turret is an element of a 3D vibrating system, which performs complex motion in relation to the $0_v x_v y_v z_v$ reference system consisting of a straightline motion of the mass centre S_v in accordance with a change in the y_v coordinate, rotary motion about the $S_v z_v$ axis in accordance with a change in the pitch angle ϑ_v and rotary motion about the $S_v x_v$ axis in accordance with a change in the tilt angle $v p_v$.

In the general case, the position of the $S_w \xi_w \eta_w \zeta_w$ coordinate system in relation to the $S_w x_w y_w z_w$ coordinate system is determined by the Bryant angles ϑ_w and φ_w. The application of these angles leads to an isometric sequential transformation $\mathbf{R}_{\vartheta_w \varphi_w}$, which is a combination of two consecutive revolutions ϑ_w and φ_w. The transformation $\mathbf{R}_{\vartheta_w \varphi_w}$ has the following form

$$\mathbf{R}_{\vartheta_w \varphi_w} = \begin{bmatrix} \cos \vartheta_w & \sin \vartheta_w & 0 \\ -\sin \vartheta_w \cos \varphi_w & \cos \vartheta_w \cos \varphi_w & \sin \varphi_w \\ \sin \vartheta_w \sin \varphi_w & -\cos \vartheta_w \sin \varphi_w & \cos \varphi_w \end{bmatrix} \qquad (1.1)$$

We consider low values of angular vibrations of the launcher pedestal, thus, if there is such a degree of approximation, we can assume that

$$\begin{aligned} \sin \vartheta_w &= \vartheta_w & \cos \vartheta_w &= 1 \\ \sin \varphi_w &= \varphi_w & \cos \varphi_w &= 1 \end{aligned}$$

and neglect the ratios of these angles.

The transformation $\mathbf{R}_{\vartheta_w \varphi_w}$ as a matrix has the following form

$$\mathbf{R}_{\vartheta_w \varphi_w} = \begin{bmatrix} 1 & \vartheta_w & 0 \\ -\vartheta_w & 1 & \varphi_w \\ 0 & -\varphi_w & 1 \end{bmatrix} \tag{1.2}$$

Generally, the position of the $S_v \xi_v \eta_v \zeta_v$ coordinate system in relation to the $S_v x_v y_v z_v$ coordinate system is determined by the Bryant angles ϑ_v and φ_v. The application of these angles leads to an isometric sequential transformation $\mathbf{R}_{\vartheta_v \varphi_v}$, which is a combination of two consecutive revolutions ϑ_v and φ_v. The transformation $\mathbf{R}_{\vartheta_v \varphi_v}$ has the following form

$$\mathbf{R}_{\vartheta_v \varphi_v} = \begin{bmatrix} \cos \vartheta_v & \sin \vartheta_v & 0 \\ -\sin \vartheta_v \cos \varphi_v & \cos \vartheta_v \cos \varphi_v & \sin \varphi_v \\ \sin \vartheta_v \sin \varphi_v & -\cos \vartheta_v \sin \varphi_v & \cos \varphi_v \end{bmatrix} \tag{1.3}$$

We consider low values of angular vibrations of the launcher turret, thus, if there is such a degree of approximation, we can assume that

$$\sin \vartheta_v = \vartheta_v \qquad \cos \vartheta_v = 1$$
$$\sin \varphi_v = \varphi_v \qquad \cos \varphi_v = 1$$

and neglect the ratios of these angles.

The transformation $\mathbf{R}_{\vartheta_v \varphi_v}$ has the following matrix form

$$\mathbf{R}_{\vartheta_v \varphi_v} = \begin{bmatrix} 1 & \vartheta_v & 0 \\ -\vartheta_v & 1 & \varphi_v \\ 0 & -\varphi_v & 1 \end{bmatrix} \tag{1.4}$$

The turret inertia characteristic is dependent on the actual position of its component objects at the moment the target is intercepted. The turret configuration is determined basing on positions of the platform and the guide rail system. The position of the platform body with mass m_{pl} and moments of inertia $I_{pl\xi'_v}$, $I_{pl\eta'_v}$, $I_{pl\zeta'_v}$ and the position of the body of the guide rail system with mass m_{pr} and moments of inertia $I_{pr\xi_{pv}}$, $I_{pr\eta_{pv}}$, $I_{pr\zeta_{pv}}$ are determined in right-handed Cartesian orthogonal coordinate systems. The reference systems are the following coordinate systems:

a) Coordinate systems defining position of the platform:

$S_v \xi'_v \eta'_v \zeta'_v$ – the coordinate system rotated about the angle ψ_{pv} in relation to the $S_v \xi_v \eta_v \zeta_v$ coordinate system. The $S_v \xi'_v$, $S_v \eta'_v$ and $S_v \zeta'_v$ axes are rigidly connected with the platform body so that they are the main central axes of inertia. The operator rotates the platform by the tilt angle ψ_{pv} in relation to the target position.

b) Coordinate systems defining position of the guide rail system:

$S_v\xi_{pv}\eta_{pv}\zeta_{pv}$ – the coordinate system rotated by ϑ_{pv} in relation to the $S_v\xi'_v\eta'_v\zeta'_v$
coordinate system. The $S_v\xi_{pv}$, $S_v\eta_{pv}$ and $S_v\zeta_{pv}$ axes are rigidly connec-
ted with the body of the system of guide rails so that they are the main
central axes of inertia. The operator rotates the platform by the pitch
angle ϑ_{pv} in relation to the target position.

The mutual position of the coordinate systems discussed above is determi-
ned by the Bryant angles ψ_{pv} and ϑ_{pv}. The application of these angles leads
to a transformation in form of a transformation matrix.

The transformation $\mathbf{R}_{\psi_{pv}}$ from the $S_v\xi_v\eta_v\zeta_v$ coordinate system to the
$S_v\xi'_v\eta'_v\zeta'_v$ coordinate system has the following form (Fig. 3)

$$\mathbf{R}_{\psi_{pv}} = \begin{bmatrix} \cos\psi_{pv} & 0 & -\sin\psi_{pv} \\ 0 & 1 & 0 \\ \sin\psi_{pv} & 0 & \cos\psi_{pv} \end{bmatrix} \tag{1.5}$$
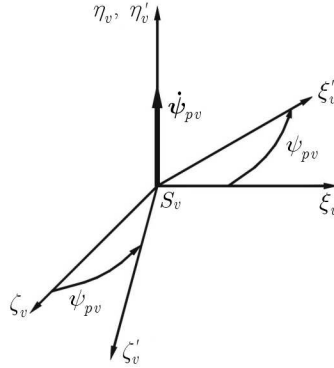
Fig. 3. Transformation of the $S_v\xi'_v\eta'_v\zeta'_v$ coordinate system in relation to the
$S_v\xi_v\eta_v\zeta_v$ coordinate system

The transformation $\mathbf{R}_{\vartheta_{pv}}$ from the $S_v\xi'_v\eta'_v\zeta'_v$ coordinate system to the
$S_v\xi_{pv}\eta_{pv}\zeta_{pv}$ coordinate system has the following form (Fig. 4)

$$\mathbf{R}_{\vartheta_{pv}} = \begin{bmatrix} \cos\vartheta_{pv} & \sin\vartheta_{pv} & 0 \\ -\sin\vartheta_{pv} & \cos\vartheta_{pv} & 0 \\ 0 & 0 & 1 \end{bmatrix} \tag{1.6}$$

The position of the $S_v\xi_{pv}\eta_{pv}\zeta_{pv}$ coordinate system in relation to the
$S_v\xi_v\eta_v\zeta_v$ coordinate system is determined by the Bryant angles ψ_{pv} and ϑ_{pv},
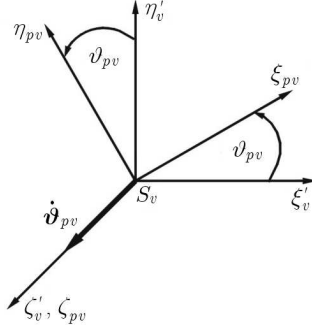
Fig. 4. Transformation of the $S_v\xi_{pv}\eta_{pv}\zeta_{pv}$ coordinate system in relation to the $S_v\xi'_v\eta'_v\zeta'_v$ coordinate system

as shown in Fig. 5. The application of these angles lead to an isometric sequential transformation $\mathbf{R}_{\psi_{pv}\vartheta_{pv}}$, which is a combination of two consecutive revolutions ψ_{pv} and ϑ_{pv}. The transformation $\mathbf{R}_{\psi_{pv}\vartheta_{pv}}$ has the following form

$$\mathbf{R}_{\psi_{pv}\vartheta_{pv}} = \begin{bmatrix} \cos\psi_{pv}\cos\vartheta_{pv} & \sin\vartheta_{pv} & -\sin\psi_{pv}\cos\vartheta_{pv} \\ -\cos\psi_{pv}\sin\vartheta_{pv} & \cos\vartheta_{pv} & \sin\psi_{pv}\sin\vartheta_{pv} \\ \sin\psi_{pv} & 0 & \cos\psi_{pv} \end{bmatrix} \qquad (1.7)$$
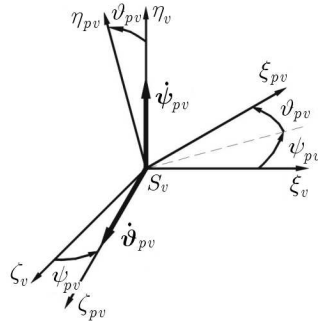
Fig. 5. Transformation of the $S_v\xi_{pv}\eta_{pv}\zeta_{pv}$ coordinate system in relation to the $S_v\xi_v\eta_v\zeta_v$ coordinate system

2. A mathematical model of the launcher of the self-propelled anti-aircraft missile system

There are six degrees of freedom resulting from the structure of the model describing disturbances to the launcher basic motion in space.

Three independent generalized coordinates were assumed to determine positions of the pedestal with mass m_w and moments of inertia I_{wx}, I_{wz} at any moment:

y_w – vertical displacement of the centre of the launcher pedestal mass S_w,

φ_w – angle of rotation of the launcher pedestal about the $S_w x_w$ axis,

ϑ_w – angle of rotation of the launcher pedestal about the $S_w z_w$ axis.

Three independent generalized coordinates were assumed to determine positions of the turret with mass m_v, moments of inertia I_{vx}, I_{vz} and moment of deviation I_{vxz} at any moment:

y_v – vertical displacement of the centre of the launcher mass S_v,

φ_v – angle of rotation of the launcher about the $S_v x_v$ axis,

ϑ_v – angle of rotation of the launcher pedestal about the $S_v z_v$ axis.

For the launcher, the equations of motion are

$$m_w \ddot{y}_w + f_{yw} = 0 \qquad I_{wz} \ddot{\vartheta}_w + f_{\vartheta w} = 0 \qquad I_{wx} \ddot{\varphi}_w + f_{\varphi w} = 0 \quad (2.1)$$

and

$$
\begin{aligned}
(m_v + m_{p1} + m_{p2} + m_{p3} + m_{p4})\ddot{y}_v + f_{yv} = 0 \\
I_{\vartheta v} \ddot{\vartheta}_v + f_{\vartheta v} = 0 \qquad I_{\varphi v} \ddot{\varphi}_v + f_{\varphi v} = 0
\end{aligned}
\quad (2.2)
$$

where

f_{yw} – function of coordinates $y_w, \vartheta_w, \varphi_w, y_v, \vartheta_v, \varphi_v, y_n, \vartheta_n, \varphi_n$ and their derivatives with respect to time, specifying the analytical form of restitution, dissipative and gravity forces, including the generalized static displacement,

$f_{\vartheta w}, f_{\varphi w}$ – function of coordinates $y_w, \vartheta_w, \varphi_w, y_v, \vartheta_v, \varphi_v, y_n, \vartheta_n, \varphi_n$ and their derivatives with respect to time, specifying the analytical form of restitution and dissipative forces moments acting in the direction of ϑ_w and vp_w coordinate, respectively, with the static generalized displacement,

f_{yv} – function of coordinates $y_w, \vartheta_w, \varphi_w, y_v, \vartheta_v, \varphi_v, \xi_{p1}, \xi_{p2}, \xi_{p3}, \xi_{p4}$ and their derivatives with respect to time, specifying the analytical form of restitution, dissipative, gravity, inertia and gyroscopic forces, taking into account the static generalized displacement,

$f_{\vartheta v}$ – function of coordinates $y_w, \vartheta_w, \varphi_w, y_v, \vartheta_v, \varphi_v, \xi_{p1}, \xi_{p2}, \xi_{p3}, \xi_{p4}$ and their derivatives with respect to time, specifying the analytical form of moments of forces restitution, dissipative, gravity, inertia and gyroscopic forces moments, taking into account the static generalized displacements,

$f_{\varphi v}$ – function of coordinates $y_w, \vartheta_w, \varphi_w, y_v, \vartheta_v, \varphi_v, \xi_{p1}, \xi_{p2}, \xi_{p3}, \xi_{p4}$ and their derivatives with respect to time, specifying the analytical form of moments of forces restitution, dissipative, gravity, inertia and gyroscopic, including the static generalized displacement,

$I_{\vartheta v}, I_{\varphi v}$ – reduced moment of inertia resulting from the movement pursuant to the coordinate ϑ_v and φ_v, respectively.

Functions $f_{yw}, f_{\vartheta w}, f_{\varphi w}, f_{yv}, f_{\vartheta v}, f_{\varphi v}$ and reduced moments of inertia $I_{\vartheta v}$, $I_{\varphi v}$ need to be written in long mathematical expressions, the analytical form of which is presented in the monograph by Dziopa (2008).

Some of the physical quantities are included in Fig. 1 and Fig. 2.

3. Numerical simulation of the launcher motion

The launcher is directly subjected to disturbances generated during the launch. Excitations caused by the launch of each of the four missiles are passed onto the pedestal through the turret. The launcher vibrations result also from the excitation generated by the vehicle moving across a battlefield. The pedestal mounted on the vehicle passes the disturbances to the turret and the missiles being launched. Examples of the angular acceleration variations for the pedestal and the turret in the pitch and tilt motions are shown in Figs. 6 and 7.
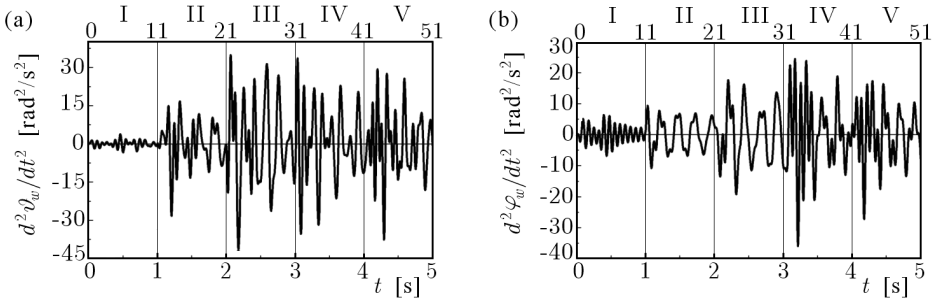
Fig. 6. Angular acceleration of the pedestal: (a) in pitch motion, (b) in tilt motion

The standard deviation of the pedestal angular acceleration in the pitch motion $\ddot{\vartheta}_w$ is $\sigma_{\ddot{\vartheta}_w} = 11.5348 \, \text{rad/s}^2$. The standard deviation of the pedestal angular acceleration $\ddot{\varphi}_w$ in the tilt motion is $\sigma_{\ddot{\varphi}_w} = 7.9355 \, \text{rad/s}^2$.

The standard deviation of the turret angular acceleration $\ddot{\vartheta}_v$ in the pitch motion is $\sigma_{\ddot{\vartheta}_v} = 28.0760 \, \text{rad/s}^2$.
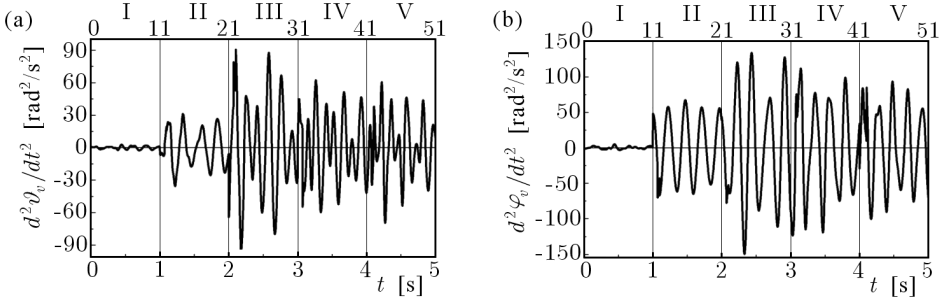
Fig. 7. Angular acceleration of the turret: (a) in tilt motion, (b) in pitch motion

The standard deviation of the turret angular acceleration $\ddot{\varphi}_v$ in the tilt motion is: $\sigma_{\ddot{\varphi}_v} = 53.9298\,\text{rad/s}^2$.

The paper presents the concept of application of a three-axis gyroscope platform mounted on the pedestal of a self-propelled anti-aircraft system with the aim of stabilizing the launcher, i.e. eliminating the undesired angular motions of the vehicle and the missiles being launched. The principle of operation of the system is presented in a schematic diagram in Fig. 8.

It is predicted that, except for the launcher, there may be another gyroscope-stabilized system fixed on the platform. This system, responsible for the space scanning and target tracking, is able to detect the target automatically while the vehicle moves. The target is then tracked until it is destroyed by one of the missiles in the anti-aircraft missile system.

4. A simplified model of motion of the three-degree gyroscope platform (TGP)

Figure 9 shows a schematic diagram of a three-axis platform equipped with two three-degree gyroscopes (Pavlov, 1954; Pavlovskiĭ, 1986). It is required that there are at least two frames of the platform: inner and outer. The platform and the frames are equipped with angular displacement sensors and transmitters of control moments (Pavlov, 1954; Pavlovskiĭ, 1986). The gyroscopes are mounted inside the platform in such a way that the measurement axes of the gyroscope are parallel to the corresponding axes of the platform frames. One gyroscope has the main axis parallel to the Ox_p axis of the platform, therefore, it is able to measure the platform rotations about the other two axes, Oy_p and Oz_p. The main axis of the other gyroscope, however, is parallel to the Oy_p axis of the platform and, therefore, it is able to measure the platform rotations about
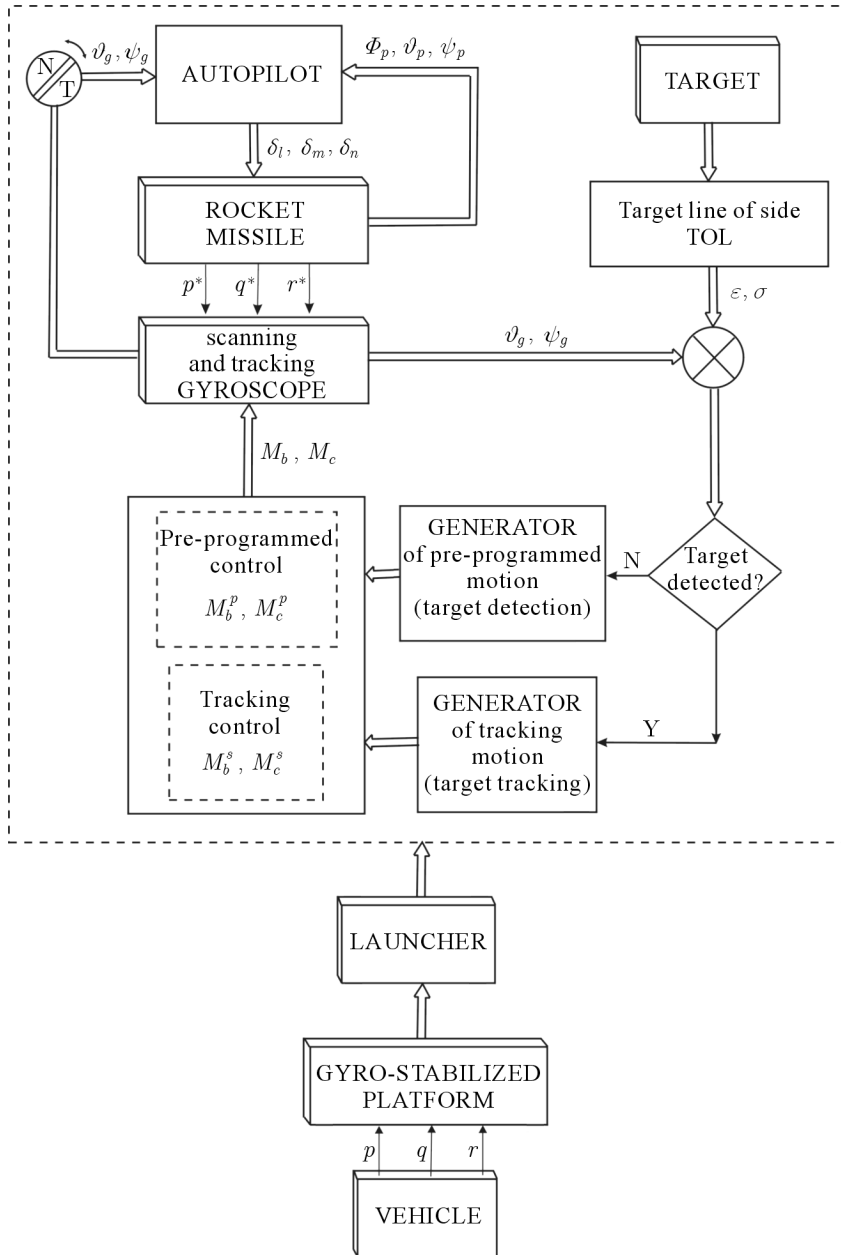
Fig. 8. Schematic diagram of the principle of operation of the self-propelled anti-aircraft missile system with a three-axis gyroscope-stabilized platform

axes Ox_p and Oz_p. In the three-axis platform, the motions about the three axes of suspension interact. The two stabilization systems affect each other, which means that if there are any disturbances to one axis, they are passed to the other two axes.
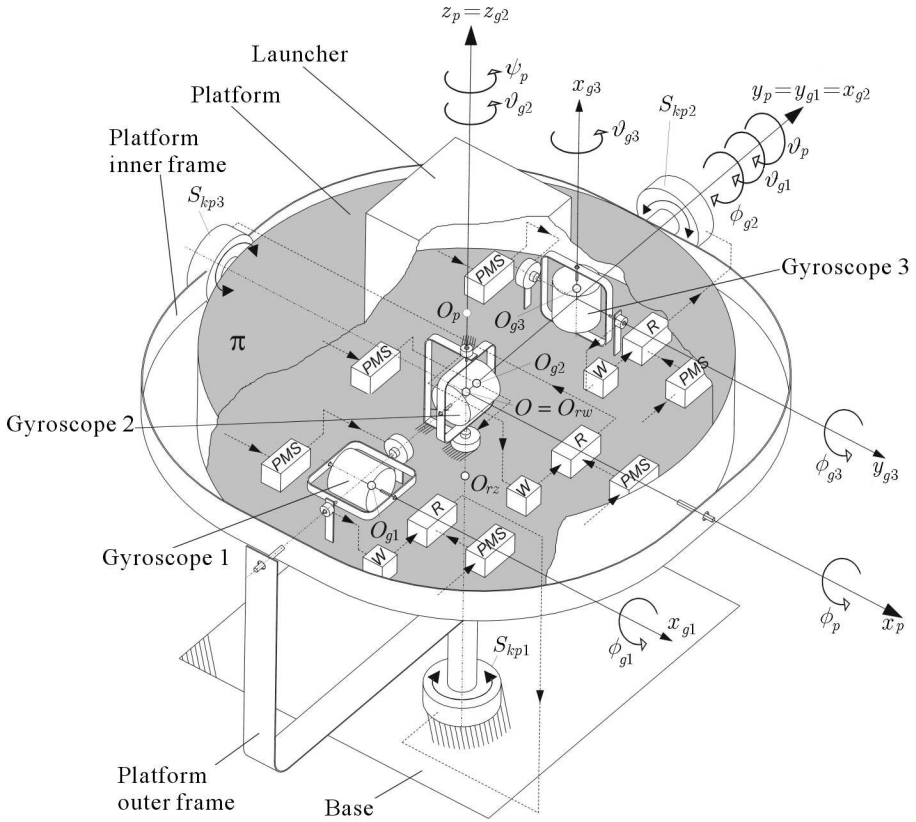
Fig. 9. General view of the three-axis gyroscope-stabilized platform mounted on a wheeled vehicle

In addition, since the platform is subjected to vibrations and other external disturbances, it is necessary that the control parameters be optimally selected both at the design stage and under operational conditions.

The model presented below describes the gyroscope platform control in a closed-loop system, where the control parameters are optimized using the LQR method (Koruba, 2001).

Due to limited space, the model is a linearized model. Let us consider a case when the angular displacements of the gyroscope axes and the platform elements from the initial positions are small. If we neglect the ratios of velo-

cities as low order quantities and assume that the gyroscopes are astatic and the inertia of their frames is negligible, we have:

— equations describing motion of the gyroscopes:

$$J_{gk}(\ddot{\vartheta}_{g1} - \ddot{\psi}_p - \dot{r}^*) + J_{go}n_{g1}(\dot{\psi}_{g1} + \dot{\vartheta}_p + q^*) = M_{kg1_2} - M_{r2_{g1}}$$

$$J_{gk}(\ddot{\vartheta}_{g2} + \ddot{\phi}_p + \dot{p}^*) + J_{go}n_{g2}(\dot{\psi}_{g2} - \dot{\psi}_p - r^*) = M_{kg2_2} - M_{r2_{g2}}$$

$$J_{gk}(\ddot{\psi}_{g1} + \ddot{\vartheta}_p + \dot{q}^*) + J_{go}n_{g1}(\dot{\psi}_p - \dot{\vartheta}_{g1} + r^*) = M_{kg1_1} - M_{r1_{g1}}$$

$$J_{gk}(\ddot{\psi}_{g2} - \ddot{\psi}_p - \dot{r}^*) + J_{go}n_{g2}(\dot{\phi}_p - \dot{\vartheta}_{g2} + p^*) = M_{kg2_1} - M_{r1_{g2}}$$

(4.1)

— equations describing motion of the platform elements (platform, inner frame, outer frame)

$$[J_{x_p} + J_{gk} + m_p l_p^2 + l_{g1p}^2(m_{1_{g1}} + m_{2_{g1}} + m_{3_{g1}}) + l_{g2p}^2(m_{1_{g2}} + m_{2_{g2}} +$$
$$+ m_{3_{g2}})](\ddot{\phi}_p + \dot{p}^*) + J_{gk}\ddot{\vartheta}_{g2} - J_{go}n_{g2}(\dot{\psi}_p + \dot{\psi}_{g2} + r^*) + V_p m_p l_p(\dot{\psi}_p + r^*) +$$
$$+ V_p(m_{1_{g1}} + m_{2_{g1}} + m_{3_{g1}})l_{g1p}(\dot{\psi}_{g1} + \dot{\vartheta}_p + q^*) +$$
$$- V_p(m_{1_{g2}} + m_{2_{g2}} + m_{3_{g2}})l_{g2p}(\dot{\vartheta}_p + q^*) = M_{kp3} - M_{rp}$$

$$(J_{y_{rw}} + J_{y_p} + J_{gk} + m_p l_p^2)(\ddot{\vartheta}_p + \dot{q}^*) + J_{gk}\ddot{\psi}_{g1} + J_{go}n_{g1}(\dot{\psi}_p - \dot{\vartheta}_{g1} + r^*) +$$
$$+ m_p l_p \dot{V}_p + V_p[-2(m_{1_{g1}} + m_{2_{g1}} + m_{3_{g1}})l_{g1p}(\dot{\phi}_p + p^*) +$$
$$+ (m_{1_{g2}} + m_{2_{g2}} + m_{3_{g2}})l_{g2p}\dot{\phi}_p] = M_{kp2} - M_{rrw}$$

(4.2)

$$[J_{z_{rz}} + J_{z_{rw}} + J_{z_p} + 2J_{gk} + l_{g1p}^2(m_{1_{g1}} + m_{2_{g1}} + m_{3_{g1}}) + l_{g2p}^2(m_{1_{g2}} + m_{2_{g2}} +$$
$$+ m_{3_{g2}})](\ddot{\psi}_p + \dot{r}^*) - J_{gk}\ddot{\vartheta}_{g1} - J_{gk}\ddot{\psi}_{g2} - J_{go}n_{g1}(\dot{\vartheta}_p + \dot{\psi}_{g1} + q^*) +$$
$$+ J_{go}n_{g2}(\dot{\phi}_p + \dot{\vartheta}_{g2} + p^*) + [l_{g1p}(m_{1_{g1}} + m_{2_{g1}} + m_{3_{g1}}) +$$
$$- l_{g2p}(m_{1_{g2}} + m_{2_{g2}} + m_{3_{g2}})]\dot{V}_p + V_p m_p l_p(\dot{\vartheta}_p - \dot{\phi}_p) = M_{kp1} - M_{rrz}$$

where J_{go}, J_{gk} are moments of inertia of the gyroscope rotors; $J_{x_p}, J_{y_p}, J_{z_p}, J_{y_{rw}}, J_{z_{rz}}$ – moments of inertia of the platform elements; $m_{1_{gi}}, m_{2_{gi}}, m_{3_{gi}}, i = 1, 2$ – masses of the rotor and the inner and outer frames of gyroscopes 1 and 2, respectively; l_p, l_{g2p}, l_{g2p} – distances between the centres of gravity of the platform, gyroscope 1, gyroscope 2 and the geometric center of platform rotation, respectively; $\vartheta_{g1}, \psi_{g1}, \vartheta_{g2}, \psi_{g2}, \phi_p, \vartheta_p, \psi_p$ – angles determining the position of particular axes of rotation of the gyroscope and platform elements; n_{g1}, n_{g2} – angular velocities of the rotors of gyroscopes 1 and 2, respectively; V_p – linear velocity of the vehicle; p^*, q^*, r^* – angular velocities of the vehicle; M_{ri} – moments of friction forces in the bearings of the axis of rotation of particular gyroscopes and platform elements; M_{kgi}, M_{kpi} – stabilization moments generated by the correction motors of the gyroscope and platform elements; respectively.

5. Optimal selection of the control parameters for the three-axis gyroscope platform on a movable base

Let us write the equations of motion of the controlled platform in the vector-matrix form

$$\dot{\boldsymbol{x}} = \mathbf{A}\boldsymbol{x} + \mathbf{B}\boldsymbol{u}_p \tag{5.1}$$

The vector $\boldsymbol{u}_p$ shows a pre-programmed open-loop control (Dziopa, 2006a), the schematic diagram of which is presented in Fig. 10.
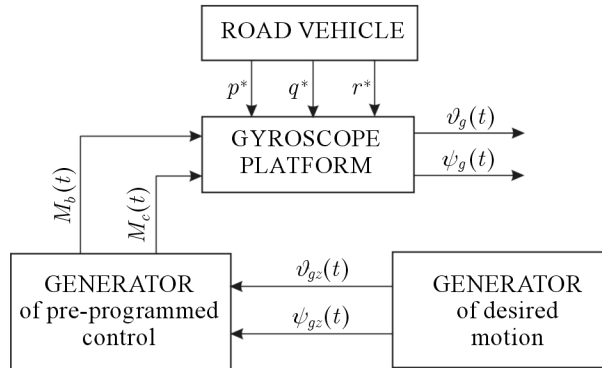
Fig. 10. Schematic diagram of control of the gyroscope platform in the open-loop system

To assure the platform stability, it is necessary to apply an additional corrective control $\boldsymbol{u}_k$ to the closed-loop system. Then, the equations describing motion of the controlled platform will become

$$\dot{\boldsymbol{x}}^* = \mathbf{A}\boldsymbol{x}^* + \mathbf{B}\boldsymbol{u}_k \tag{5.2}$$

where: $\boldsymbol{x}^* = \boldsymbol{x} - \boldsymbol{x}_p$ is the deviation between the real and desired motions; $\boldsymbol{x}_p$ is the desired vector of state of the analyzed gyroscope platform.

The law of stabilization control $\boldsymbol{u}_k$ is determined by using the linear-square optimization LQR method (Koruba, 2001) with a functional in the form

$$J = \int_0^\infty [(\boldsymbol{x}^*)^\top \mathbf{Q}\boldsymbol{x}^* + \boldsymbol{u}_k^\top \mathbf{R}\boldsymbol{u}_k]\, dt \tag{5.3}$$

The law is presented in the following form

$$\boldsymbol{u}_k = -\mathbf{K}\boldsymbol{x}^* \tag{5.4}$$
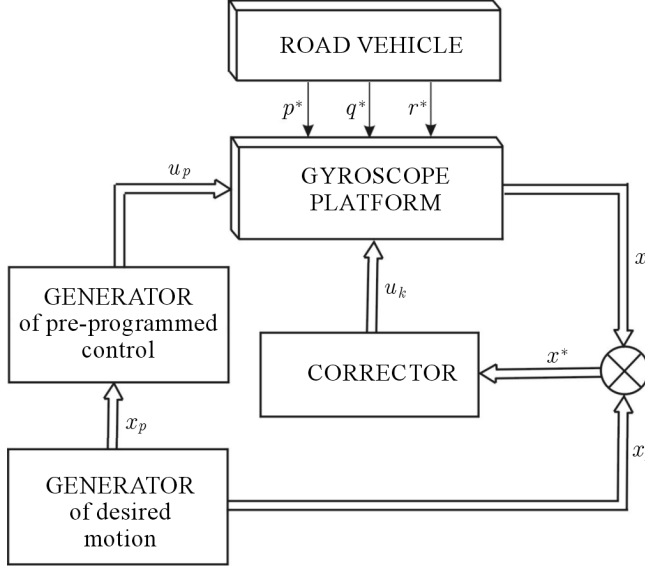
Fig. 11. Schematic diagram of control of the gyroscope platform in the closed-loop
system

where

$$\boldsymbol{u} = [M_{k1}, M_{ki+1}, M_{kk}]^\top$$
$$\boldsymbol{x} = [\psi_{g1}, \dot{\psi}_{g1}, \vartheta_{g1}, \dot{\vartheta}_{g1}, \psi_{g2}, \dot{\psi}_{g2}, \vartheta_{g2}, \dot{\vartheta}_{g2}, \dot{\Phi}_p, \dot{\vartheta}_p, \dot{\psi}_p]^\top$$
$$\boldsymbol{x}_p = [\psi_{g1z}, \dot{\psi}_{g1z}, \vartheta_{g1z}, \dot{\vartheta}_{g1z}, \psi_{g2z}, \dot{\psi}_{g2z}, \vartheta_{g2z}, \dot{\vartheta}_{g2z}, \dot{\Phi}_{pz}, \dot{\vartheta}_{pz}, \dot{\psi}_{pz}]^\top$$

The coupling matrix $\mathbf{K}$ found in Eq. (5.4) is derived from the following
relationship

$$\mathbf{K} = \mathbf{R}^{-1}\mathbf{B}^\top\mathbf{P} \tag{5.5}$$

The matrix $\mathbf{P}$ is a solution to the algebraic Riccati equation

$$\mathbf{A}^\top\mathbf{P} + \mathbf{P}\mathbf{A} - 2\mathbf{P}\mathbf{B}\mathbf{R}^{-1}\mathbf{B}^\top\mathbf{P} + \mathbf{Q} = \mathbf{0} \tag{5.6}$$

In Eqs. (5.5) and (5.6), the matrices of weights $\mathbf{R}$ and $\mathbf{Q}$ reduced to the
diagonal form are matched experimentally; the search begins at equal values

$$q_{ii} = \frac{1}{2x_{i_{max}}} \qquad\qquad r_{ii} = \frac{1}{2u_{i_{max}}} \qquad\qquad i = 1, 2, \ldots, n \tag{5.7}$$

where $x_{i_{max}}$ is the maximum range of changes in the i-th value of the state
variable, $u_{i_{max}}$ – maximum range of changes in the i-th value of the control
variable.

Figure 12 presents a simplified schematic diagram of the control and correction of the three-axis gyroscope platform.
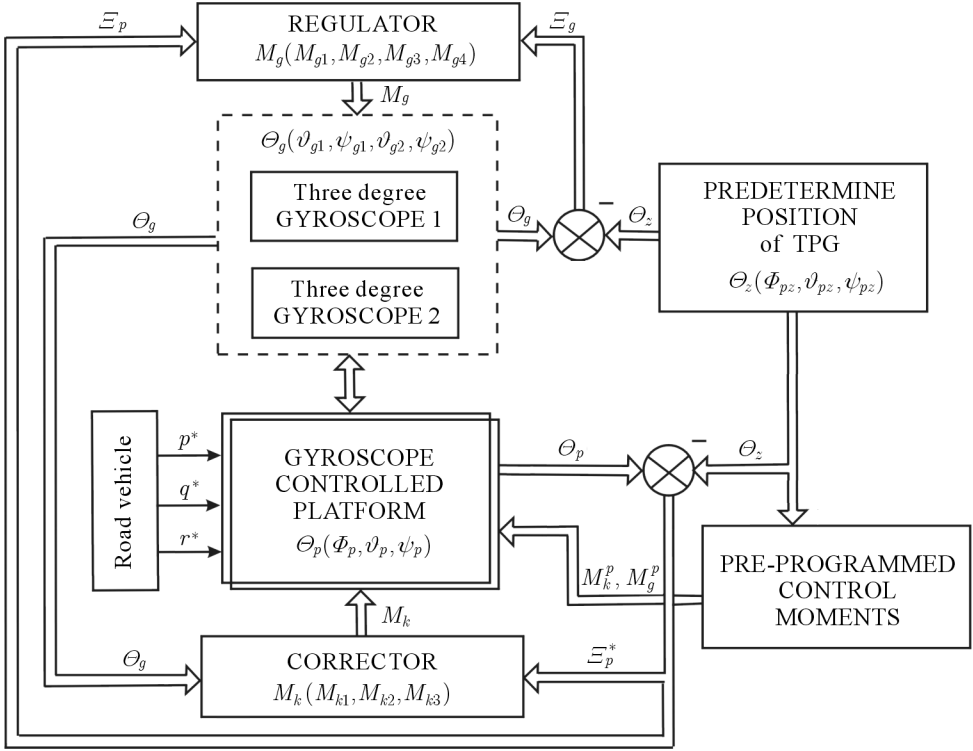
Fig. 12. Schematic diagram of control of a TGP in the open-loop system

6. Results

Figures 13-20 show the performance of the stabilization platform. There is a clear difference in the system operation resulting from the parameter selection.

Figures 17 and 18 show the performance of the platform affected by kinematic excitations of the pedestal. The dynamics is illustrated in Figs. 6 and 7. Corrective controls clearly protect the platform from the influence of the pedestal.

When a disturbance occurs, the platform remains in the transitional process for a relatively long period of time, if the selection of the regulator parameters is not optimal. However, if the regulator parameters are optimized with the LQR method, the platform returns to the initial position immediate-
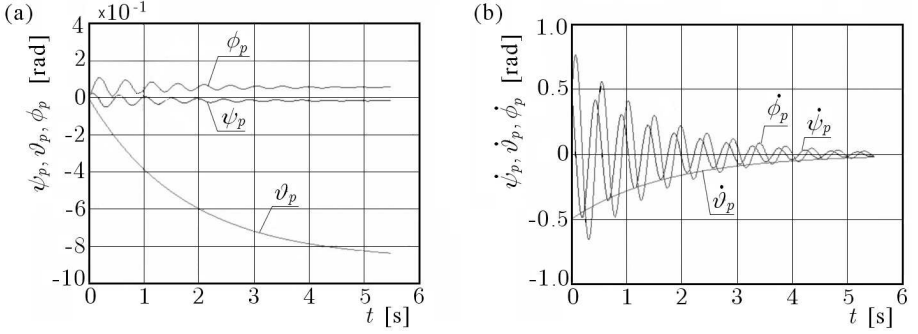
Fig. 13. Displacements of the platform for the initially selected parameters of regulators, (a) time-dependent angular displacements, (b) time-dependent changes in angular velocities
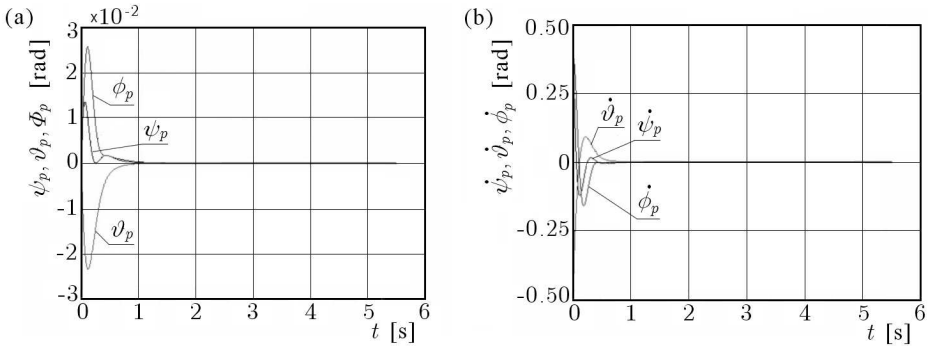
Fig. 14. Angular displacements of the platform for the optimized parameters of regulators, (a) time-dependent angular displacements, (b) time-dependent changes in angular velocities
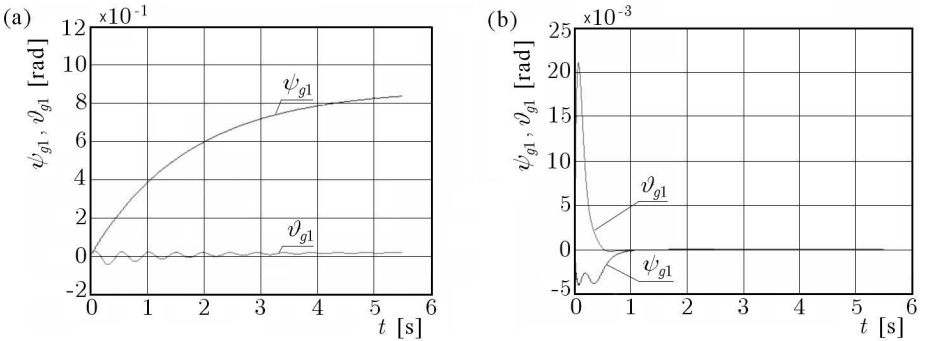
Fig. 15. Angular displacements of gyroscope 1 (a) for the initially selected parameters of regulators, (b) for the optimized parameters of regulators

(a)

(b)
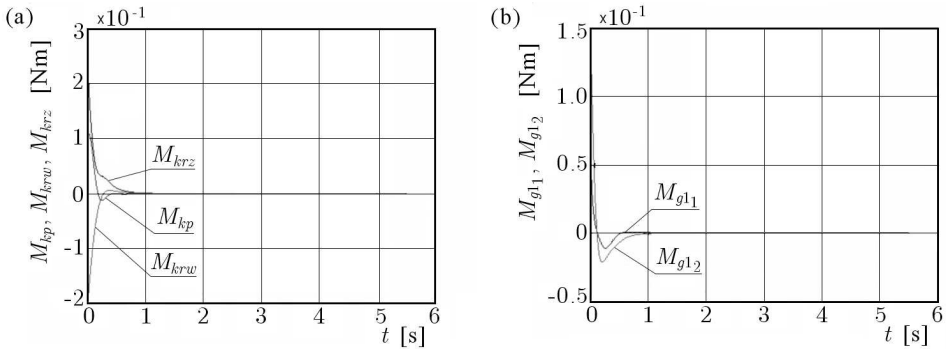
Fig. 16. Optimized correction moments of (a) the platform, (b) gyroscope 1

(a)

(b)
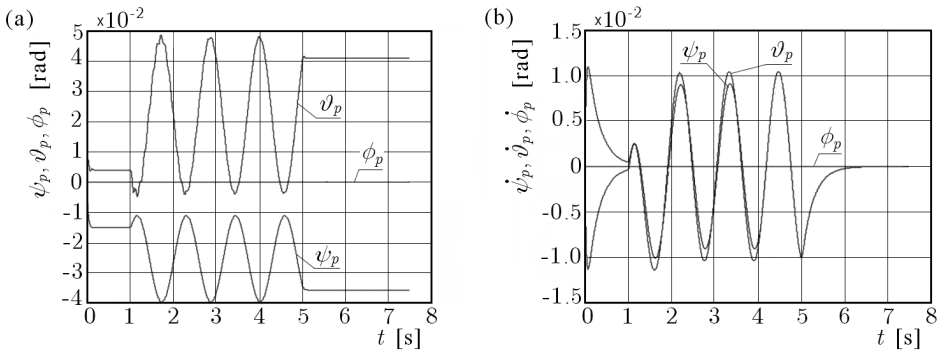
Fig. 17. Time-dependent angular displacements due to kinematic motion of the pedestal, (a) without corrective controls, (b) with corrective controls

(a)

(b)
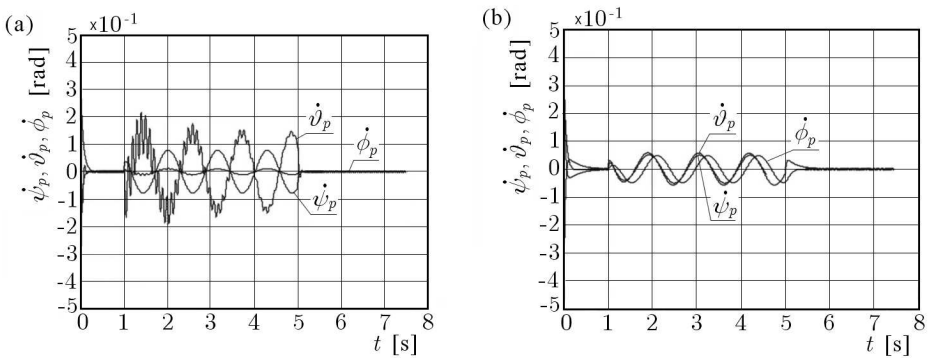
Fig. 18. Time-dependent changes in angular velocities resulting from kinematic motion of the pedestal (a) without corrective controls, (b) with corrective controls
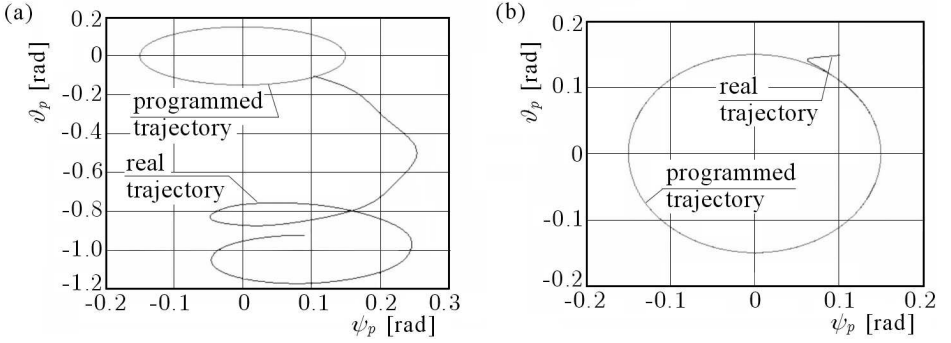
Fig. 19. Pre-programmed motion of the platform around a circular cone (a) for the initially selected parameters of regulators, (b) for the optimized parameters of regulators
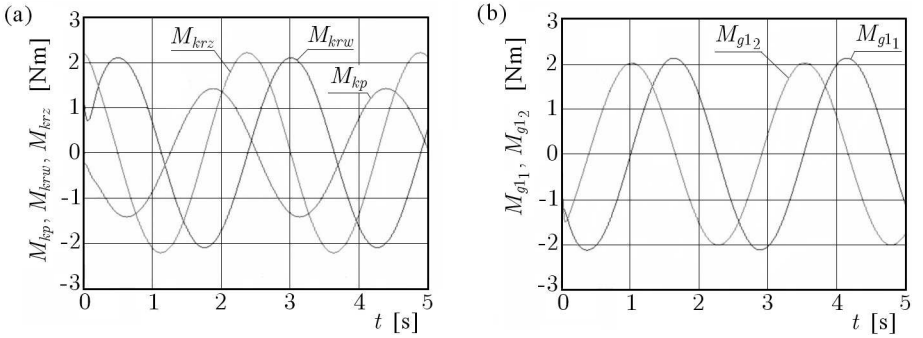
Fig. 20. Optimized correction moments in pre-programmed motion of (a) the platform, (b) gyroscope 1

ly (Fig. 14). Similar variations of the angular quantities and their derivatives in function of time can be observed for the platform gyroscopes (Fig. 15). It should be emphasized that the values of the optimized correction moments of the platform and one of the gyroscopes are relatively small (Fig. 16).

As can be seen in Figs. 19 and 20, the platform moves in a pre-programmed motion around a circular cone. Figure 19 shows the pre-determined and real trajectories in the coordinates ψ_p and ϑ_p. If the parameters of regulators are optimized, only the initial phase of the platform operation does not coincide with the pre-determined one, which is due to external disturbances. After a short period of time, the platform performs a pre-programmed motion. Figure 20 shows a diagram of correction moments generated by the stabilization motors of the platform and gyroscope 1, so that the platform can perform the pre-programmed motion.

Rererences

1. Dziopa Z., 2004, The dynamics of a rocket launcher placed on a self-propelled vehicle, *Mechanical Engineering*, **81**, 3, 23-30, ISSN 1729-959

2. Dziopa Z., 2005, An analysis of physical phenomena generated during the launch of a missile from an anti-aircraft system, *The Prospects and Development of Rescue, Safety and Defense Systems in the 21st Century*, Polish Naval Academy, Gdynia, ISBN, 83-87280-78-X, 296-303

3. Dziopa Z., 2006a, An anti-aircraft self-propelled system as a system determining the initial parameters of the missile flight, *Mechanics in Aviation ML-XII 2006*, PTMTS, ISBN 83-902194-6-8, 223-241

4. Dziopa Z., 2006b, Modelling an anti-aircraft missile launcher mounted on a road vehicle, *Theory of Machines and Mechanisms*, Vol. 1, University of Zielona Góra and PKTMiM, ISBN 83-7481-043-2, 205-210

5. Dziopa Z., 2006c, The missile coordinator system as one of the objects of an anti-aircraft system, *6th International Conference on Armament Technology: Scientific Aspects of Armament Technology*, Military University of Technology, ISBN 83-89399-27-X, 221-229

6. Dziopa Z., 2008, *The Modelling and Investigation of the Dynamic Properties of the Sel-Propelled Anti-Aircraft System*, Kielce University of Technology, Kielce

7. Koruba Z., 2001, *Dynamics and Control of a Gyroscope on Board of an Flying Vehicle*, Monographs, Studies, Dissertations No. 25. Kielce University of Technology, Kielce [in Polish]

8. Koruba Z., Osiecki J., 1999, *Construction, Dynamics and Navigation of Close-Range Missiles*, Part 1, University Course Book No. 348, Kielce University of Technology Publishing House, PL ISSN 0239-6386, Kielce [in Polish]

9. Mishin V.P. (edit.), 1990, *Dinamika raket*, Mashinostroenie, Moskva

10. Mitschke M., 1977, *Dynamics of a Motor Vehicle*, WKŁ, Warszawa [in Polish]

11. Pavlov V.A., 1954, *Abiacionnye giroskopicheskie pribory*, Gos. Izdat. Oboronnoǐ Primyshlennosti, Moskva

12. Pavlovskiǐ M.A., 1986, *Teoriya giroskopov*, Byshcha Shkola, Kiev

13. Svetlickiǐ V.A., 1963, *Dinamika starta letatel'nykh apparatob*, Nauka, Moskva

Dynamika i sterowanie platformy giroskopowej s samobieżnym zestawie przeciwlotniczym

Streszczenie

W pracy przedstawiony jest model matematyczny trzyosiowej platformy giroskopowej na ruchomej podstawie (pojeździe samochodowym). Sterowania programowe platformy wyznaczone są z zadnia odwrotnego dynamiki, natomiast sterowania korekcyjne – za pomocą metody LQR. Rozpatrywana platforma może znaleźć zastosowanie jako niezależna pdstawa dla układów obserwacyjnych, kamer, działek czy też karabinie maszynowych. W niniejszym opracowaniu pokazane jest jej zastosowanie do stabilizacji wyrzutni przeciwlotniczych pocisków rakietowych.